Mouse CHD4-NURD is required for spermatogonia survival and normal meiotic progression.

Rodrigo O. de Castro[*], Paola Onate-Colobon[*], Luciana Previato[*], Agustin Carbajal[*], Victor Goitea[*], Courtney T. Griffin[†,‡], and Roberto J. Pezza[*,‡,§].

[*]Cell Cycle and Cancer Biology Research Program, Oklahoma Medical Research Foundation, Oklahoma City, Oklahoma, United States of America.

[†]Cardiovascular Biology Research Program, Oklahoma Medical Research Foundation, Oklahoma City, Oklahoma, United States of America.

[‡]Department of Cell Biology, University of Oklahoma Health Science Center, Oklahoma City, Oklahoma, United States of America.

[§]Corresponding author: Roberto J. Pezza. Suite B305. 825 NE 13th street, Oklahoma City, Oklahoma, 73104. Tel. 405-271-6467. Email: pezzar@omrf.org.

Running title: CHD4-NURD function in gametogenesis

Key words: mouse gametogenesis, spermatogonia, meiosis, and NURD.

Abstract

Testis development and sustained germ cell production in adults rely on the establishment and maintenance of spermatogonia stem cells and their proper differentiation into spermatocytes, which through two consecutive cell divisions produce mature gametes. The chromatin remodeling complexes regulate critical processes in both premeiotic and meiotic stages of gamete development by restricting or promoting accessibility of DNA repair and gene expression machineries to the chromatin. Here, we investigated the role of the NUcleosome Remodeling and Deacetylase (NURD) complex during spermatogenesis. Our cellular and biochemical analyses revealed differential expression and composition of NURD subunits in germ cells at different stages of testis development. Germ cell-specific deletion early in gametogenesis of the NURD catalytic component Chd4, but not Chd3, resulted in arrested early gamete development due to failed cell survival of neonate undifferentiated spermatogonia stem cell population. Candidate assessment revealed that CHD4 controls Dmrt1 and its downstream target Plzf, both described as prominent regulators of spermatogonia stem cell maintenance. Further, deletion of Chd4 at meiotic relevant stages of gamete development resulted in spermatocyte arrest at a zygotene-like stage, with apparent deficient double-strand break repair and abnormal homologous chromosome synapsis. Together, our results uncover a dual requirement of CHD4 in mammalian gametogenesis and point to unique functions for the NURD complex with respect to other chromatin remodelers during gamete development.

Introduction

Defects in gametogenesis are a leading cause of infertility and an important cause of birth defects associated with aneuploidy. Insights into the mechanisms underlying testis

formation, including spermatogonia stem cell and spermatocyte development, are necessary to improve the outcomes of common gonad developmental diseases.

In mice, spermatogenesis begins from isolated germ cells called spermatogonia A-singles (As) that undergo to a series of mitotic divisions to produce spermatogonia known as paired (Apr) and aligned (Aal) that contains chains of 4 to16 cells anchored by intercellular bridges as a result of with incomplete cytokinesis [1, 2]. At this point, spermatogonia cells start a process of differentiation (A1, A2, A3, A4 or intermediate (In)), formation of type B spermatogonia, and then transition to pre-leptotene cells that initiate the series of meiotic divisions that ultimately originate spermatozoa.

Meiotic recombination in eukaryotes is initiated by double-stand breaks promoted by the SPO11 protein [3]. This is followed by the nucleolytic resection of 5′ DNA at the break site to produce a 3′ ssDNA overhang. These DNA repair intermediates are used by DMC1 and RAD51 recombinases to perform homology search to identify the allelic locus on the other parental chromosome. After strand invasion, a series of intermediates are formed and resolved culminating in the formation of chiasmata (the cytological manifestation of crossovers), which is required for stable association of the homologous chromosome pairs [4]. Closely related to the formation and repair of double-strand breaks, the maternal and paternal homologous chromosomes find each other (chromosome pairing) and form stable contacts by forming the synaptonemal complex (chromosome synapsis) [5]. Synaptonemal complex formation starts at the prophase stage of leptotene. Later, in zygotene, the homologous chromosomes begin to zipper together to form the tripartite synaptonemal complex, and it is fully assembled in pachytene. Cells remain in pachytene until checkpoints that monitor recombination and synapsis are satisfied. Upon pachytene exit, the synaptonemal complex disassembles as the meiotic cell progresses through diplotene.

Chromatin undergoes extensive remodeling during gametogenesis, leading to altered gene expression and chromosome organization, and ultimately controlling obligatory developmental transitions such as the conversion from undifferentiated to differentiated spermatogonia, spermatogonia commitment to meiosis, and meiotic progression [6, 7]. The NURD (NUcleosome Remodeling and Deacetylase) is a prominent chromatin modifying complex that functions to control gene expression via chromatin remodeling and histone deacetylation [8, 9]. The NURD complex contains two highly conserved and widely expressed catalytic subunits, CHD3/Mi-2α (chromodomain-helicase-DNA-binding 3) and CHD4/Mi-2β, which are members of the SNF2 superfamily of ATPases [8-12]. A third NURD member, CHD5, has also been described to function in the testis [13]. NURD plays a central role in various developmental and cellular events, such as controlling the differentiation of stem cells, maintaining cell identity, and responding to DNA damage [12, 14, 15]. In testis, CHD5 is required for normal spermiogenesis and proper spermatid chromatin condensation, while CHD3/4 has been described to localize at the X-Y pseudoautosomal region, the X centromeric region, and then spreads into the XY body chromatin [16, 17]. Although the role of CHD5 has been well defined, no studies to date have addressed the requirements or mechanisms of CHD4 and CHD3 in any germ cell type.

In this study, we report that CHD4 (but not CHD3) is essential for testis development and sustained germ cell production. Germ cell-specific deletion of CHD4 results in the developmental arrest of undifferentiated spermatogonia in neonatal mice progressing to the Sertoli-only phenotype. Our studies of selected CHD4 target genes and subsequent cytological and expression analysis show that CHD4 control Dmrt1 gene expression and downstream targets such as Plzf. We propose this one of the mechanisms

by which CHD4 contributes to early germ cell development by regulating genes that are required for survival/maintenance of spermatogonia cells. Deletion of Chd4 in cells undergoing meiosis resulted in impaired meiotic progression, which cytologic cause can be ascribed to double-strand break repair defects and abnormal homologous chromosome synapsis. This study shows the requirement of CHD4 and the NURD complex in regulating gamete development in both pre-meiotic and meiotic stages of development.

Results

Chd4 expression during mouse germ cell development

To investigate a potential role for CHD4 in germ cells, we assessed CHD4 expression in newborn and adult mouse testes by immunofluorescence. CHD4 was highly expressed in spermatogonia cells (marked by PLZF, aka ZBTB16) and in Sertoli cells (marked by SOX9) (Fig. 1A and Fig. S1), but not in the negative control (PLZF-positive spermatogonia from Ddx4-*Chd4*$^{-/-}$ testes, Fig. S2A). PLZF is expressed in undifferentiated spermatogonia [18, 19]. In pachytene cells, the nuclear immunosignal of CHD4 is located mostly at the sex body (Fig. 1B). In agreement with a previous report [16], immunosignal of CHD4 was detected in late-pachytene stages associated to the pseudoautosomal region of the X-Y chromosomes (Fig. 1A, selected area on adult mouse top panel, and Fig. 1B). In sum, CHD4 is detected in spermatogonia, Sertoli cells, and primary spermatocytes.

We confirmed that CHD4 is expressed at both pre-meiotic and meiotic stages of male gamete development by analyzing CHD4 protein levels by western blot in enriched fractions (see methods for details) of undifferentiated and differentiating spermatogonia (obtained from wild type 7dpp mice and using THY1.2+ and c-KIT+ affinity columns, respectively, Fig. S3) and pachytene cells. CHD4 was also detected in the affinity column flowthrough (which was enriched mostly in Sertoli cells, here demonstrated by

immunoblotting of Sox9), and in another preparation enriched in pachytene spermatocytes (Fig. 1C). The level of cell population enrichment was assessed by western blot and markers specific for undifferentiated spermatogonia (PLZF), differentiating spermatogonia (STRA8), and primary spermatocytes (SYCP3) (Fig. 1C). Our results are comparable to those published by Bergs, et. al. [16].

Composition of CHD4-NURD complexes during spermatogenesis

NURD function is influenced by its subunit composition [20, 21]. To determine whether the expression of NURD composition might change during spermatogenesis, first we analyzed the levels of representative NURD subunits in enriched fractions of undifferentiated and differentiating spermatogonia, the flow-through after spermatogonia enrichment, and pachytene spermatocytes. Although NURD subunits HDAC2A, MTA1, RBBP4, RBBP7 and MBD2 were present in enriched fractions of undifferentiated (THY1.2+) and differentiating (c-KIT+) spermatogonia, the levels of MTA1, RBBP7, and MBD2 subunits were substantially reduced in pachytene spermatocytes (Fig. 1C), suggesting a particular composition and perhaps a different function for CHD4-NURD in this cell type.

To determine the composition of CHD4-NURD complexes, we used co-immunoprecipitation analysis to uncover NURD subunits that interact with CHD4 in enriched fractions of THY1.2 plus c-KIT spermatogonia cells and the flow-through. The NURD subunits HDAC2A, MTA1, and RBBP4/RBBP7, but not MBD2, coimmunoprecipitated with CHD4 from all fractions (Fig. 1D). HDAC2A coimmunoprecipitated with CHD4 from wild type and *Chd3*$^{-/-}$ spermatogonia cells (Fig. S2B). These data suggest that: i) CHD4 forms a NURD complex independently of CHD3, ii) that loss of CHD3 does not perturb CHD4-NURD complex formation in spermatogonia cells.

Deletion of *Chd4* but not *Chd3* results in testis developmental defects

To examine the potential functions of *Chd4* and *Chd3* during spermatogenesis, we generated a series of *Chd4* and *Chd3* germline conditional knockout mice (Fig. 2A-D). To delete the floxed allele in gonocytes (embryonic day 15.5, Fig. 2C) [22], male Ddx4-Cre; $Chd4^{WT/\Delta}$ were crossed with $Chd4^{fl/fl}$ females to generate Ddx4-Cre; $Chd4^{fl/\Delta}$ conditional knockout mice (here called Ddx4-$Chd4^{-/-}$). A similar strategy was used to generate Ddx4-$Chd3^{-/-}$ mice (Fig. 2B). We confirmed deletion of *Chd3* and *Chd4* by RT-qPCR (Fig. 2D) and immunolabeling of CHD4 (Fig. S2A).

Ddx4-$Chd4^{-/-}$ adult mice (2 months old) appeared normal in all aspects except in the reproductive tissues. Testes were significantly smaller in Ddx4-$Chd4^{-/-}$ males (mean: 0.017g ± SD: 0.005, number of quantified mice n=4 (8 testes), P≤0.0001, t test) compared to wild type (0.104 g ± 0.015, n=6 mice (12 testes)) littermates (Fig. 2E), indicating severe developmental defects in the testis.

We found that adult Ddx4-$Chd4^{-/-}$ males develop testicular hypoplasia with hyperplasia of interstitial cells and lack spermatozoa (Fig. 3A). The number of seminiferous tubules is similar between wild type and mutant animals, but the diameter is reduced (wild type, mean ± SD, 287 ± 34, n=400 seminiferous tubules cross sections (3 different mice, 2-month-old) versus $Chd4^{-/-}$ 148 ± 21.3, n=210, P<0.0001 t test).

Analysis of Ddx4-$Chd4^{-/-}$ testes revealed a total loss of germ cells (marked by TRA98) in seminiferous tubules (Fig. 3B). No developing gametes were observed, including cell types at early stages (e.g., spermatogonia) (Fig. 3A and B). Sertoli cells develop normally in Ddx4-$Chd4^{-/-}$ mice, consistent with the specific loss of *Chd4* in germ cells at early stages of development. We did not observe differences in germ cell development between wild type and Ddx4-$Chd3^{-/-}$ mice (Fig. S4A), consistent with their similar testis sizes (Fig. 2E).

We also analyzed H&E-stained histological sections of ovaries from 45-day-old wild type and Ddx4-*Chd4*$^{-/-}$ female mice. We noted a significant reduction in ovary size, an increase in stromal cells, a reduced number of follicles (wild type, 10 ± 3, n=6 mice versus Ddx4-*Chd4*$^{-/-}$ 0.6 ± 0.9, n=5, P<0.0001 t test) and absent corpora lutea (wild type, 9 ± 1, n=6 mice versus Ddx4-*Chd4*$^{-/-}$ 0 ± 0, n=5, P<0.0001 t test) in the Ddx4-*Chd4*$^{-/-}$ mice compared to wild type (Fig. 3C).

We conclude that deletion of *Chd3* has no apparent effect on gamete development. However, germ cell specific deletion of *Chd4* results in severe male and female germ cell developmental defects, possibly originated at premeiotic stages of development.

CHD4 is required for neonate spermatogonia survival

The severe phenotypes observed in Ddx4-*Chd4*$^{-/-}$ mice (Fig. 2 and 3) prompted us to investigate spermatogonial differentiation during testis development in newborns. Testis sections from 9 dpp Ddx4-*Chd4*$^{-/-}$ mice stained with H&E showed a markedly reduced number of germ cells (Fig. 4A) as well as differences in cell composition, compared to those from age-matched wild type mice. To analyze this in detail, we examined the presence of cells expressing STRA8 (Fig. 4A), which marks differentiating spermatogonia, SYCP3 and yH2AX which are markers of primary spermatocytes and TRA98, a marker for germ cells (Fig. S5). Whereas tubules from 9 dpp wild type mice contained cells expressing TRA98 (45 ± 10, n=66 seminiferous tubules counted obtained from 3 mice) and STRA8 (18.8 ± 8.4, n=36 obtained from 3 mice), tubules from *Chd4*$^{-/-}$ mice showed a near absence of cells expressing these markers (TRA98 4.6 ± 3, n=60 obtained from 3 mice, P<0.0001, t test; STRA8 2.5 ± 3.5, n=42 obtained from 3 mice, P<0.0001, Student t test) (Fig. 4A). Testes sections from 9 dpp *Chd4*$^{-/-}$ mice also showed a reduction in primary spermatocytes expressing the meiotic prophase I markers SYCP3 and γH2AX compared to those from 9 dpp wild type mice (Fig. S5A and B). Together, the results

further suggest that testis defects in *Chd4*$^{-/-}$ mice begin early, during pre-meiotic stages of postnatal development, leading to an absence of germ cells in adults.

To pinpoint when the testes defects originate in *Chd4*$^{-/-}$ mice, we stained testes sections from 1-21dpp mice for the expression of PLZF/ZBTB16 (undifferentiated neonate spermatogonia [18, 19]) and TRA98 (all germ cells). Compared to wild type, *Chd4* mutant sections displayed a small reduction in the number of cells expressing TRA98 at both 1dpp and 3dpp (Fig. 4B and 4C and Fig. S6). We observed equal numbers of SOX9-positive Sertoli cells in testes from wild type and *Chd4*$^{-/-}$ mice at 3, 4, and 7 dpp (Fig. 4C), as expected for the specific loss of *Chd4* in spermatogonia cells. Both PLZF-positive and TRA98-positive cells were substantially reduced in *Chd4*$^{-/-}$ testis compared to wild type testis at 4 dpp and 7dpp (Fig. 4C).

Given that Chd4 may act as a regulator of cell-cycle progression, we then examined whether the rapid loss of PLZF-positive neonate spermatogonia in *Chd4*$^{-/-}$ testes was due to altered proliferative activity. We conducted EdU incorporation study to test this possibility. 4dpp mice were injected with EdU and analyzed 3 h later, after which we assayed its incorporation in PLZF-positive spermatogonia in whole mounts of seminiferous tubules (Fig. S7A). We found that spermatogonia cell proliferation (PLZF/EdU^{+} cells) in wild type and Ddx4-Chd4$^{-/-}$ is proportionally the same (Fig. S7C). In addition, reduced amount of total PLZF-positive cells was found in Ddx4-CHD4$^{-/-}$ compared to wild type in the whole-mounting experiment (Fig. S7B).

To determine whether cell death contributed to the loss of Ddx4-*Chd4*$^{-/-}$ neonate spermatogonia (Fig. 4C), we performed TUNEL assay in staining paraffin embedded testis sections of wild type and *Chd4*$^{-/-}$ four days old testis. At this age the testis is mostly constituted by spermatogonia and Sertoli cells, which can be easily distinguished by DAPI

nuclear staining patterns. We found a significant increase in the percentage of apoptotic cells in *Chd4*$^{-/-}$ testis compared to wild type mice (Fig. 4D).

We conclude that the possible cause of spermatogonia failure in *Chd4*$^{-/-}$ mice is in the survival/maintenance of neonate undifferentiated spermatogonia.

CHD4, DMRT1, and PLZF work together in a regulatory axis involved in spermatogonia cell survival

Our results show that CHD4 is required for spermatogonia maintenance/survival. We then reason that CHD4 may interact with genes that have been described to work in spermatogonia maintenance. Indeed, DMRT1 has been show to function in spermatogonia stem cells maintenance, and this function seems to be mediated by direct regulation of Plzf gene expression, another transcription factor required for spermatogonia maintenance [23]. To test our hypothesis, we immunostained paraffined testes sections from 1, 4, and 7 dpp mice for the presence of DMRT1 (Fig. 5A and B). Compared to wild type, *Chd4* mutant showed a clear reduction in DMRT1 immunosignal.

Recent work described that Dmrt1 controls Plzf expression, which is a transcription factor required for spermatogonia maintenance [23]. We then tested the effect of CHD4 depletion in Plzf expression. PLZF immunostaining of testes sections from 1, 4, and 7 dpp mice revealed a significantly reduction of this protein in Chd4 knockout cells respect to wild type (Fig. 5C and D). This is consistent with a model by which CHD4 control of Dmrt1 and downstream targets influences cell survival/maintenance (Fig. 5E).

We concluded that Chd4 participates in the maintenance/survival of neonate spermatogonia stem cell possibly through transcriptional regulation of genes participating in these critical processes. We note, however, that the dramatic phenotype observed in CHD4$^{-/-}$ spermatogonia likely reflect CHD4 targeting a wide spectrum of genes participating in different pathways.

CHD4 is required for normal completion of meiosis

Our results using Ddx4-Cre mice have demonstrated that Chd4 is essential in pre-meiotic phases of spermatogenesis making it unfeasible to study possible functions of Chd4 during meiosis. Thus, to bypass the early requirements of Chd4, we generated Ngn3-*Chd4*$^{-/-}$ and SPO11-*Chd4*$^{-/-}$ germline conditional knockout mice. Because we observed incomplete depletion of CHD4 when Spo11-Cre was used (Fig. S8), this strain was not further analyzed. Ngn3-*Chd4*$^{-/-}$ adult mice (2 months old) appeared normal in all aspects except in the reproductive tissues. Testes were significantly smaller in Ngn3-*Chd4*$^{-/-}$ males (mean: 0.026g ± SD: 0.003, number of quantified mice n=4 (8 testes), P≤0.0001, t test) compared to wild type (0.100 g ± 0.008, n=6 mice (12 testes)) littermates (Fig. 6A and B), indicating severe developmental defects in the testis. We confirmed deletion of *Chd4* by western blot and immunofluorescence (Fig. 6C and D, respectively).

Analysis of H&E-stained testis sections revealed that gametogenesis progresses trough initial stages of prophase I, but cells are arrested in a zygotene-like stage (Fig. 6A), consistent with an effect specific for meiotic stages of development. The Ngn3-*Chd4*$^{-/-}$ mutant testes showed signs of extensive apoptosis in seminiferous tubules with approximately 95% of TUNEL positive cells (142 seminiferous tubules scored) at the zygotene-like stage (Fig. 6E). We also analyzed H&E-stained histological sections of ovaries from 2-month-old wild type and Ngn3-*Chd4*$^{-/-}$ female mice. We noted no significant different regarding ovary size, changes in stromal cells, or reduced number of follicles in the mutant respect to wild type (Fig. 6F).

To assess male meiosis I defects in detail, we analyzed spermatocyte progression through meiotic prophase I by scoring individual stages of asynchronous populations of wild type and Ngn3-*Chd4*$^{-/-}$ spermatocytes from adult mice (Fig. 7A and B). We observed

a significant increase in pachytene cells in Ngn3-*Chd4*$^{-/-}$ knockout versus wild type (70.8 ± 4.9%, n = 165 total cells from 3 mice versus 42.3 ± 10.1%, n = 233 total cells from 4 mice; P≤0.0043, two tailed t test) and a decrease in diplotene spermatocytes when knockout is compared to wild type (12.3 ± 6.1%, cells vs. 52.7 ± 16.4%; P ≤ 0.0053).

In sum, independent of its role in spermatogonia, CHD4 is required for normal mouse meiotic progression.

DSB repair is apparently defective in CHD4 mice

CHD4 is known to play a role in the DNA damage response in somatic cells [9, 24, 25]. For example, *Chd4* knockdown results in increased γH2AX, a marker of double-strand breaks, and CHD4 accumulates at sites of DNA damage [7]. To determine whether CHD4 is required to repair the programmed double-strand breaks that occur in germ cells during meiosis, we immunostained spermatocyte chromosome spreads for γH2AX, a marker of DNA damage. In agreement with a mid-meiotic arrest, the repair of double-stand breaks in chromosomes evaluated by the γH2AX signal outside the sex body appeared impaired in Ngn3-*Chd4*$^{-/-}$ spermatocytes compared to wild type mice (57.2 ± 23.2%, n = 4 mice versus 0.33 ± 0.57%, n = 3 mice; mean ± SD; P = 0.009, two tailed t test) (Fig. 7A and C).

***CHD4* mutants exhibit defects in homologous chromosome synapsis of autosomes**

During meiotic prophase, the association of the homologous chromosome pairs is stabilized by the synaptonemal complex. Homologous synapsis can be monitored by following the immunosignal of proteins of the lateral element (e.g., SYCP3) and the central region (e.g., SYCP1) on chromosome spread preparations. A detailed analysis of Ngn3-*Chd4*$^{-/-}$ spermatocytes revealed abnormal formation of the synaptonemal complex (wild type 2.90 ± 5.02%, n = 3 mice versus Ngn3-*Chd4*$^{-/-}$ 37.50 ± 10.01%, n = 4 mice; mean ±

SD; P = 0.0017, two tailed t test, Fig. 7D). Homologous synapsis initiation appeared normal in Ngn3-*Chd4*$^{-/-}$ spermatocytes, as judged by staining patterns for SYCP3 and SYCP1 in leptonema cells, but proper pachynema with fully synapsed autosomal bivalents was rarely observed (Fig. 7A). Instead, the most advanced cells showed a late zygotene-like morphology (full-length axes have been developed and synapsis is near complete) but with characteristics of pachytene cells such as acquisition of the characteristic knob-like accumulation of SYCP3 at telomeres (Fig. 7A). Because there does not appear to be a stage when synapsis is complete, it is likely that the unsynapsed regions we observe correspond to chromosomal areas that never synapsed. Together with synaptic defects, a high proportion of Ngn3-*Chd4*$^{-/-}$ spermatocytes show SYCP3 aggregates compared to wild type (21 ± 14.17%, n = 3 mice versus 1.33 ± 2.30%, n = 3 mice; mean ± SD)

We concluded that Ngn3-*Chd4*$^{-/-}$ spermatocytes exhibit incomplete synapsis, a characteristic that likely triggers cell arrest and apoptosis.

Discussion

In this work, we examined the potential function of two critical NURD catalytic subunits, CHD4 and CHD3, in spermatogenesis. Our data suggest that a CHD4-NURD (but not CHD3-NURD) complex controls neonate spermatogonia development at early stages of testis development (Fig. 8). Germline deletion of *Chd4,* but not *Chd3,* results in a severe loss of germ cells specifically at early stages of the testis cord development. *Chd4* deletion affects spermatogonia, with the first obvious consequences in undifferentiated spermatogonia.

Most CHDs are expressed in testis; however, their insertion into the NURD complex seems to be developmentally regulated, with different patterns of expression during gametogenesis. CHD5 [10-12] has been shown to be expressed and required to

compact chromatin in postmeiotic stages of spermatogenesis [13, 26]. Our results show that CHD4 is expressed and functions at premeiotic and meiotic stages of gametogenesis.

The functions of CHD4-NURD in neonate spermatogonia development and male gametogenesis are further revealed by our cytological analysis showing that CHD4 regulates the expression of Dmrt1 (Fig. 5). DMRT1 function in maintenance of spermatogonia stem cells has been proposed to be mediated by direct regulation of Plzf gene expression, another transcription factor required for spermatogonia maintenance [23]. In agreement with this possibility, we observed that the amount of PLZF was significantly reduced in Chd4 knockout versus wild type cells. In sum, our work provides evidence of a regulatory axis in which CHD4 may control important genes involved in spermatogonia stem cell maintenance and survival. Additional work will be required to test CHD4 effect in Sohlh1, another Dmrt1 direct target involved in cell survival and differentiation [23, 27, 28], and the Stra8 gene, the latter which precocious expression is detected in Dmrt1 knockout mice. We note that the dramatic cellular phenotype we observed after CHD4 depletion in spermatogonia may be only explained by CHD4 activity targeting several genes and different pathways.

We also observed that CHD4 is essential for progression of normal meiosis in the mouse. Using cytological methods, we determined that spermatocyte development arrest occurs at mid stages of meiosis I prophase with failure in both DNA repair and homologous chromosome synapsis. Deficient repair of double strand breaks in CHD4 knockout spermatocytes is not surprising as CHD4 has been directly implicated in the response to damaged DNA in somatic cells models. Indeed, CHD4 is recruited to artificially generated DNA damage sites and affects DNA repair through different pathways [11, 25, 29, 30]. For example, CHD4 recruits the BRIT1 protein to influence RPA and BRCA1 loading on DNA damage sites [10]. CHD4 also interacts with MCPH1 and its loss interferes with the

recruitment of MCPH1 to damage sites [7]. Importantly, MCPH1 regulates the recruitment of RPA, RAD51 and BRCA2 to DSB sites undergoing recombination repair. Given its positive impact on survival following irradiation, current models predict that CHD4 promotes a permissive chromatin environment for proper DSB repair [9, 11, 29], a model that well could explain the phenotype we observed. Together, our results suggest an essential role for the CHD4 ATPase in mammalian male meiosis. However, because the demonstrated vast spectrum of CHD4 possible functions in DNA repair and other important meiotic processes it is difficult to pinpoint the specific molecular causes of meiotic DNA repair failure in the model we study.

Ngn3-*Chd4*$^{-/-}$ mice exhibit an interesting phenotype regarding homologous chromosome synapsis. Evaluated by SYCP3 and SYCP1 immunostaining, the most advanced spermatocytes showed fully developed axes, but the homologous pairs remained incompletely synapsed. Although failure in DNA repair may explain the observed phenotype, it is also possible that CHD4 effect on gene expression, such as on components of the synaptonemal complex, may explain the origin of synaptic defects in Ngn3-*Chd4*$^{-/-}$ spermatocytes knockout cells.

Chromatin remodeling complexes are a vast group of regulators with diverse functions in critical cellular processes such as transcription and DNA metabolism. They have been generally classified into four different families SWI/SNF, INO80, ISWI, and NURD. Most of the knowledge we have regarding their functions come from studies of somatic cultured cell models. More recently, however, work from different labs has begun exploring the role of chromatin remodelers in germ cell development. Germline-specific deletion of *Brg1 or Brd7* [31-34] both components of the SWI/SNF complex, results in gonadal developmental defects. Deletion of *Ino80* in mouse spermatocyte resulted in a similar phenotype to that described for loss of SWI/SNF, about meiotic prophase I failure

in recombination and homologous chromosome associations [32, 35]. On the contrary, ISWI and CHD5 [36-38], the latter an alternative catalytic subunit of NURD complexes, function late in germ cell development with postmeiotic phenotypes associated with spermiogenesis and fertilization. Collectively, our studies show the unique cellular and molecular requirements of CHD4-NURD in premeiotic and meiotic stages of gamete development. These results support a model in which distinct chromatin remodeling complexes fulfill specific requirements during different stages of gamete development.

Material and Methods

Mice

CHD4-floxed mice (*CHD4*$^{fl/fl}$) have been described [39]. *Chd3*-floxed mice were generated by Cyagen Biosciences using homologous recombination of a targeting vector in C57Bl/6 embryonic stem cells. The targeting vector incorporated a 5' LoxP site inserted between exons 12 and 13 and a 3' LoxP site inserted between exons 20 and 21 of the wild type *Chd3* allele. Transgenic *Cre* recombinase mice *Ddx4-Cre*$^{\text{FVB-Tg(Ddx4-cre)1Dcas/J}}$ was purchased from The Jackson Laboratory (Bar Harbor, ME). Ngn3-Cre$^{\textbf{FVB(Cg)-Tg(Neurog3-cre)C1Able/J}}$ was purchased from The Jackson Laboratory (Bar Harbor, ME). *Chd3 or Chd4* gonad-specific knockouts and wild-type heterozygotes littermates were obtained from crosses between female homozygous *flox/flox* mice with male heterozygous Cre/+; *Chd3* Wt/flox and/or *Chd4* Wt/flox mice.

All experiments conformed to relevant regulatory standards guidelines and were approved by the Oklahoma Medical Research Foundation-IACUC (Institutional Animal Care and Use Committee).

Mice Genotyping

Characterization of wild type and *floxed* alleles was carried out by PCR using the following oligonucletides: CHD3 forward 5'-GGGTGGAGGTGGAAAGTGTA, CHD3 reverse 5'-AGAGGACAGGTCACAGGACAA, CHD4 forward 5'- TCCAGAAGAAGACGGCAGAT and CHD4 reverse 5'- CTGGTCATAGGGCAGGTCTC. The presence of *cre* recombinase allele were determine by PCR using the following primers: DDX4-Cre forward 5'-CACGTGCAGCCGTTTAAGCCGCGT, DDX4-Cre reverse 5'-TTCCCATTCTAAACAACACCCTGAA. Ngn3-Cre detection was performed using the following primer set: mutant Reverse 5'-ACA TGT CCA TCA GGT TCT TGC, common forward 5'-GGC ACA CAC ACA CCT TCC A, wild type Reverse 5'-AGT CAC CCA CTT CTG CTT CG (Transgene = ~150 bp, Wt = 197 bp). Also, standard Cre PCR genotyping used the following primers: 5'- TGCAACGAGTGATGAGGTTC and 5'-ATTCTCCCACCGTCAGTACG.

Real time-PCR

Total RNA was isolated from adult testis or from enriched fractions of spermatogonia with the Direct-zol RNA MiniPrep Plus kit (Zymo Research). RNA (2.0µg) was oligo-dT primed and reverse-transcribed with the high-capacity RNA-to-cDNA kit (Applied Biosystems). Exon boundaries of *Chd4 and Chd3* were amplified using TaqMan Assays (Applied Biosystems) as directed by the manufacturer using Beta-2 macroglobulin as standard. TaqMan Mm01190896_m1 (Chd4), Mm01332658_m1 (Chd3), and Mm00437762_m1 (Beta-2 microglobulin). Gene expression was normalized with respect to wild type with wild type expression levels considered to be 1.

Western blot cell lysates

Total testis or enriched cells fractions were lysed in ice-cold protein extraction buffer containing 0.1% Nonidet P-40, 50 mM Tris-HCl, pH 7.9, 150 mM NaCl, 3 mM MgCl2, 3 mM EDTA, 10% glycerol, 1 mM DTT, 1mM PMSF and protease inhibitors (ThermoFisher Scientific, A32965) followed by sonication (3 pulses of 10 seconds) using micro ultrasonic cell disrupter (Kontes). The relative amount of protein was determined measuring absorbance at 260nm using NanoDrop 2000c spectrophotometer (ThermoFisher Scientific). Proteins were solubilized with 2X sample buffer (4% SDS, 160 mM Tris-HCl, pH 6.8, 20% glycerol, 4% mM β-mercaptoethanol, and 0.005% bromphenol blue) and 30 μg/lane of sample were separated by 4–15% gradient Tris-acetate SDS-PAGE and electro transferred to PVDF membrane (Santa Cruz Biotechnology, sc-3723). The blots were probed with individual primary antibodies, and then incubated with HRP-conjugated goat anti-mouse or rabbit antibody as required. In all blots, proteins were visualized by enhanced chemiluninescence and images acquired using Western Blot Imaging System c600 (Azure Biosystems). ImageJ software were used for quantification of non-saturated bands and α-tubulin were used for normalization. Antibodies used are detailed in table S6.

Histology and immunostaining

Testes and ovaries were dissected, fixed in 10% neutral-buffered formalin (Sigma) and processed for paraffin embedding. After sectioning (5–8-μm), tissues were positioned on microscope slides and analyzed using hematoxylin and eosin using standard protocols. For immunostaining analysis, tissue sections were deparaffinized, rehydrated and antigen was recovered in sodium citrate buffer (10 mM Sodium citrate, 0.05% Tween 20, pH 6.0) by heat/pressure-induced epitope retrieval. Incubations with primary antibodies were carried out for 12 h at 4°C in PBS/BSA 3%. Primary antibodies used in this study are detailed in table S6 Following three washes in 1 X PBS, slides were incubated for 1 h at

room temperature with secondary antibodies. A combination of fluorescein isothiocyanate (FITC)-conjugated goat anti-rabbit IgG (Jackson laboratories) with Rhodamine-conjugated goat anti-mouse IgG and Cy5-conjugated goat anti-human IgG each diluted 1: 450 were used for simultaneous triple immunolabeling. Slides were subsequently counterstained for 3 min with 2µg/ml DAPI containing Vectashield mounting solution (Vector Laboratories) and sealed with nail varnish. We use Zen Blue (Carl Zeiss, inc.) for imaging acquisition and processing.

Cytology

We employed established experimental approaches for the visualization of chromosomes in chromosome surface spreads [40]. Incubations with primary antibodies were carried out for 12 h at 4 °C in 1× PBS plus BSA 2%. Following three washes in 1 X PBS, slides were incubated for 1 h at room temperature with secondary antibodies. A combination of fluorescein isothiocyanate (FITC)-conjugated goat anti-rabbit IgG (Jackson laboratories) with Rhodamine-conjugated goat anti-mouse IgG and Cy5-conjugated goat anti-human IgG each diluted 1:350 was used for simultaneous immunolabeling if required. Slides were subsequently counterstained for 3 min with 2 µg/ml DAPI containing Vectashield mounting solution (Vector Laboratories) and sealed with nail varnish. We used Zen Blue (Carl Zeiss, Inc.) for imaging acquisition and processing.

Primary spermatocyte enrichment

Synchronized pachytene spermatocytes from the first spermatogenic wave were purified as described in [41]. Briefly, 2 dpp mice were injected for seven consecutive days with WIN18,446 to arrest germ cells as spermatogonia. The next day (9 dpp), mice were injected with retinoic acid (RA) to induce their coordinated maturation. 2 Mice were killed at 13 days after RA injection (22 dpp). Testes were disaggregated using proteases and

meiocytes were then purified by fluorescence activated cell sorting (FACS). Unlike Romer et al, after testes disaggregation and prior to FACS, cells were not washed (by centrifugation and resuspension) to avoid breakage of fragile pachytene cells. Instead, cells were sorted from the protease-containing buffer. Purity and stage of cells was assessed by immunofluorescence of chromosome spreads using anti SYCP1 and anti SYCP3 antibodies. More than 80% of cells were at pachytene stage.

Enrichment of Spermatogonia Populations

Our procedure of cell enrichment followed [42, 43]. Briefly, testis from 7dpp mice (or any other indicated age) were removed from mice and placed in a Petri dish containing Dulbecco's Modified Eagle Medium (DMEM without phenol red). After detachment of the tunica albuginea, the seminiferous tubules were loosen using forceps and incubated in a 15 ml tube containing DMEM containing 1 mg/mL of collagenase, 300 U/mL of hyaluronidase and 5 mg/mL DNAse I (StemCell Technologies) under gentile agitation for 10 min. The seminiferous tubule clumps were pelleted by gravity and the cell suspension containing interstitial cells was discarded. The tubules were then incubated of with 0.05% Trypsin-EDTA solution (Mediatech Inc) for 5 min and the reaction was stopped by adding 10% volume of 10% BSA in PBS. Single cell suspension was obtained by mechanical resuspension followed by filtration through a 40-µm-pore-size cell strainer and dead cells were removed using Dead Cell Removal Kit (Miltenyi Biotec 130-090-101). Differentiating c-KIT+ neonate spermatogonia cells were magnetically labeled with CD117 (c-KIT+) MicroBeads (Miltenyi Biotec 130-091-224) and isolated using MS columns (Miltenyi Biotec 130-042-201) according to manufacturer’s instructions. After the depletion of the c-KIT+ cells, the population of undifferentiated neonate spermatogonia cells were separated using CD90.2 (THY1.2+) MicroBeads (Miltenyi Biotec 130-121-278). Relative enrichment of cell populations was evaluated by STRA8 (c-Kit fractions) or PLZF (THY1.2 fractions)

western blots (Fig. 1C). After c-kit and THY1.2 separation, the flow-through mostly contained Sertoli cells (SOX9 positive, Fig. 1C). The number of cells obtained from a pool of 4 mice testis at 7dpp was approximately $3.43x10^5$ in THY1.2 fractions and $5.71x10^5$ in c-Kit fractions.

Immunoprecipitation

Co-immunoprecipitation experiments were performed using testis of wild type or Ddx4-CHD3$^{-/-}$ mouse (Adult - 2 months old). After detunication, seminiferous tubules were loosen using forceps, washed twice with cold PBS and lysed using ice-cold RIPA buffer (50mM Tris pH 7.5, 150mM NaCl, 1% NP40, 0.5% Deoxycholate) containing protease inhibitors (ThermoFisher Scientific, A32965), sheared using 23G needle, incubated on ice for 15 min and centrifugated at 1000xg for 10 minutes at 4ºC. Supernatant were collected in a separate tube, the pellet were resuspended in RIPA buffer, disrupted by sonication (3 pulses of 10 seconds) and centrifuged 12.000xg. This second supernatant was combined with the previous one and protein concentration was determined. We used 1mg of protein for each immunoprecipitation. Lysates were pre-cleared with protein G magnetic beads (BioRad, 161-4023) for 1 hour at room termperature and incubated with rabbit anti-CHD3 (5µg, Bethyl A301-220A), rabbit anti-CHD4 (2µg, Abcam ab72418), or rabbit IgG (5µg Jackson ImmunoResearch, 011-000-003). Lysates were rotated overnight at 4ºC and immune complexes were collected with protein G magnetic beads (2 hours at 4ºC). Beads were washed 4 times with washing buffer (50mM Tris pH 7.5, 150mM NaCl, 0.1% TX100, 5% glycerol) and two times with PBS. Proteins were eluted by boiling the beads with 2X sample buffer and analyzed by SDS-PAGE as described above.

EdU-based proliferation assay

Mice at indicated age received subcutaneous injection of EdU (50 mg/Kg) (Invitrogen, A10044) 3 hours prior euthanasia. After that, testes were removed and processed for whole-mount immunohistochemistry. EdU was detected by incubation of testis samples with reaction mix (2mM $CuSO_4$, 50 mM ascorbic acid and 2mM Alexa Azide conjugates (488 or 647) in PBS) for 3 hours at room temperature.

Whole-mount seminiferous tubules

Immunohistochemistry of whole-mount seminiferous tubules was performed as described [44]. Briefly, after detachment of the tunica albuginea, the seminiferous tubules were loosen using forceps and incubated in a 15 ml tube containing DMEM containing 1 mg/mL of collagenase, 300 U/mL of hyaluronidase and 5 mg/mL DNAse I (StemCell Technologies) under gentile agitation for 10 min. The seminiferous tubules clumps were pelleted by gravity and the cell suspension containing interstitial cells was discarded. Seminiferous tubules were fixed for 4h in 4 % PFA (pH7.2 in PBS) at 4 ºC. After extensively wash in PBS, the tubules were permeabilized with series of MeOH/PBS (25, 50, 75, 95 %, and twice in 100 % MeOH) for 15 min at room temperature, treated with MeOH:DMSO:H_2O_2 (4:1:1), and rehydrated with MeOH/PBS (50, 25% and twice in PBS). Samples were incubated in ice-cold blocking solution PBSMT (PBS with 2% non-fat dry milk and 0.5% triton X-100) for 3 hours and then over-night at 4ºC with indicated primary antibodies under gentle rotation. Seminiferous tubules were washed in PBSMT (5 x 1h) and incubated with dye conjugated (Alexa488 or TRITC) goat anti-mouse or rabbit antibody as required. The tubules were mounted in raised coverslips glass slides.

Statistical Analyses

Results are presented as mean ± standard deviation (SD). Statistical analysis was performed using Prism Graph statistical software. Two-tailed unpaired Student's □-test

was used for comparisons between 2 groups. $P < 0.05$ was considered statistically significant.

Acknowledgments. We thank Angela Andersen from Life Science Editors editorial services for her assistance in manuscript writing.

References

1. Greenbaum MP, Yan W, Wu MH, Lin YN, Agno JE, Sharma M, et al. TEX14 is essential for intercellular bridges and fertility in male mice. Proc Natl Acad Sci U S A. 2006;103(13):4982-7. Epub 2006/03/22. doi: 10.1073/pnas.0505123103. PubMed PMID: 16549803; PubMed Central PMCID: PMCPMC1458781.
2. Phillips BT, Gassei K, Orwig KE. Spermatogonial stem cell regulation and spermatogenesis. Philos Trans R Soc Lond B Biol Sci. 2010;365(1546):1663-78. doi: 10.1098/rstb.2010.0026. PubMed PMID: 20403877; PubMed Central PMCID: PMCPMC2871929.
3. Keeney S, Giroux CN, Kleckner N. Meiosis-specific DNA double-strand breaks are catalyzed by Spo11, a member of a widely conserved protein family. Cell. 1997;88(3):375-84.
4. Sansam CL, Pezza RJ. Connecting by breaking and repairing: mechanisms of DNA strand exchange in meiotic recombination. FEBS J. 2015;282(13):2444-57. doi: 10.1111/febs.13317. PubMed PMID: 25953379; PubMed Central PMCID: PMCPMC4573575.
5. Kleckner N. Meiosis: how could it work? Proc Natl Acad Sci U S A. 1996;93(16):8167-74. PubMed PMID: 8710842.
6. Wang L, Xu Z, Khawar MB, Liu C, Li W. The histone codes for meiosis. Reproduction. 2017;154(3):R65-R79. doi: 10.1530/REP-17-0153. PubMed PMID: 28696245.
7. Stanley FK, Moore S, Goodarzi AA. CHD chromatin remodelling enzymes and the DNA damage response. Mutat Res. 2013;750(1-2):31-44. doi: 10.1016/j.mrfmmm.2013.07.008. PubMed PMID: 23954449.
8. Goodarzi AA, Kurka T, Jeggo PA. KAP-1 phosphorylation regulates CHD3 nucleosome remodeling during the DNA double-strand break response. Nat Struct Mol Biol. 2011;18(7):831-9. doi: 10.1038/nsmb.2077. PubMed PMID: 21642969.
9. Larsen DH, Poinsignon C, Gudjonsson T, Dinant C, Payne MR, Hari FJ, et al. The chromatin-remodeling factor CHD4 coordinates signaling and repair after DNA damage. J Cell Biol. 2010;190(5):731-40. doi: 10.1083/jcb.200912135. PubMed PMID: 20805324; PubMed Central PMCID: PMCPMC2935572.
10. Pan MR, Hsieh HJ, Dai H, Hung WC, Li K, Peng G, et al. Chromodomain helicase DNA-binding protein 4 (CHD4) regulates homologous recombination DNA repair, and its deficiency sensitizes cells to poly(ADP-ribose) polymerase (PARP) inhibitor treatment. J Biol Chem. 2012;287(9):6764-72. doi: 10.1074/jbc.M111.287037. PubMed PMID: 22219182; PubMed Central PMCID: PMCPMC3307306.

11. Polo SE, Kaidi A, Baskcomb L, Galanty Y, Jackson SP. Regulation of DNA-damage responses and cell-cycle progression by the chromatin remodelling factor CHD4. EMBO J. 2010;29(18):3130-9. doi: 10.1038/emboj.2010.188. PubMed PMID: 20693977; PubMed Central PMCID: PMCPMC2944064.
12. Clapier CR, Cairns BR. The biology of chromatin remodeling complexes. Annu Rev Biochem. 2009;78:273-304. doi: 10.1146/annurev.biochem.77.062706.153223. PubMed PMID: 19355820.
13. Zhuang T, Hess RA, Kolla V, Higashi M, Raabe TD, Brodeur GM. CHD5 is required for spermiogenesis and chromatin condensation. Mech Dev. 2014;131:35-46. doi: 10.1016/j.mod.2013.10.005. PubMed PMID: 24252660; PubMed Central PMCID: PMCPMC3965579.
14. Torchy MP, Hamiche A, Klaholz BP. Structure and function insights into the NuRD chromatin remodeling complex. Cell Mol Life Sci. 2015;72(13):2491-507. doi: 10.1007/s00018-015-1880-8. PubMed PMID: 25796366.
15. Eisen JA, Sweder KS, Hanawalt PC. Evolution of the SNF2 family of proteins: subfamilies with distinct sequences and functions. Nucleic Acids Res. 1995;23:2715-23.
16. Bergs JW, Neuendorff N, van der Heijden G, Wassenaar E, Rexin P, Elsasser HP, et al. Differential expression and sex chromosome association of CHD3/4 and CHD5 during spermatogenesis. PLoS One. 2014;9(5):e98203. Epub 2014/05/23. doi: 10.1371/journal.pone.0098203. PubMed PMID: 24849318; PubMed Central PMCID: PMCPMC4029951.
17. Broering TJ, Alavattam KG, Sadreyev RI, Ichijima Y, Kato Y, Hasegawa K, et al. BRCA1 establishes DNA damage signaling and pericentric heterochromatin of the X chromosome in male meiosis. J Cell Biol. 2014;205(5):663-75. Epub 2014/06/11. doi: 10.1083/jcb.201311050. PubMed PMID: 24914237; PubMed Central PMCID: PMCPMC4050732.
18. Costoya JA, Hobbs RM, Barna M, Cattoretti G, Manova K, Sukhwani M, et al. Essential role of Plzf in maintenance of spermatogonial stem cells. Nat Genet. 2004;36(6):653-9. Epub 2004/05/25. doi: 10.1038/ng1367. PubMed PMID: 15156143.
19. Buaas FW, Kirsh AL, Sharma M, McLean DJ, Morris JL, Griswold MD, et al. Plzf is required in adult male germ cells for stem cell self-renewal. Nat Genet. 2004;36(6):647-52. Epub 2004/05/25. doi: 10.1038/ng1366. PubMed PMID: 15156142.
20. Margolin G, Khil PP, Kim J, Bellani MA, Camerini-Otero RD. Integrated transcriptome analysis of mouse spermatogenesis. BMC Genomics. 2014;15:39. doi: 10.1186/1471-2164-15-39. PubMed PMID: 24438502; PubMed Central PMCID: PMCPMC3906902.
21. Nitarska J, Smith JG, Sherlock WT, Hillege MM, Nott A, Barshop WD, et al. A Functional Switch of NuRD Chromatin Remodeling Complex Subunits Regulates Mouse Cortical Development. Cell Rep. 2016;17(6):1683-98. doi: 10.1016/j.celrep.2016.10.022. PubMed PMID: 27806305; PubMed Central PMCID: PMCPMC5149529.
22. Gallardo T, Shirley L, John GB, Castrillon DH. Generation of a germ cell-specific mouse transgenic Cre line, Vasa-Cre. Genesis. 2007;45(6):413-7. Epub 2007/06/07. doi: 10.1002/dvg.20310. PubMed PMID: 17551945; PubMed Central PMCID: PMC2597027.
23. Zhang T, Oatley J, Bardwell VJ, Zarkower D. DMRT1 Is Required for Mouse Spermatogonial Stem Cell Maintenance and Replenishment. PLoS Genet. 2016;12(9):e1006293. Epub 2016/09/02. doi: 10.1371/journal.pgen.1006293. PubMed PMID: 27583450; PubMed Central PMCID: PMCPMC5008761.
24. Smeenk G, Wiegant WW, Vrolijk H, Solari AP, Pastink A, van Attikum H. The NuRD chromatin-remodeling complex regulates signaling and repair of DNA damage. J Cell Biol. 2010;190(5):741-9. doi: 10.1083/jcb.201001048. PubMed PMID: 20805320; PubMed Central PMCID: PMCPMC2935570.

25. Qi W, Chen H, Xiao T, Wang R, Li T, Han L, et al. Acetyltransferase p300 collaborates with chromodomain helicase DNA-binding protein 4 (CHD4) to facilitate DNA double-strand break repair. Mutagenesis. 2016;31(2):193-203. doi: 10.1093/mutage/gev075. PubMed PMID: 26546801.
26. Li W, Wu J, Kim SY, Zhao M, Hearn SA, Zhang MQ, et al. Chd5 orchestrates chromatin remodelling during sperm development. Nat Commun. 2014;5:3812. doi: 10.1038/ncomms4812. PubMed PMID: 24818823; PubMed Central PMCID: PMCPMC4151132.
27. Matson CK, Murphy MW, Griswold MD, Yoshida S, Bardwell VJ, Zarkower D. The mammalian doublesex homolog DMRT1 is a transcriptional gatekeeper that controls the mitosis versus meiosis decision in male germ cells. Dev Cell. 2010;19(4):612-24. Epub 2010/10/19. doi: 10.1016/j.devcel.2010.09.010. PubMed PMID: 20951351; PubMed Central PMCID: PMCPMC2996490.
28. Suzuki H, Ahn HW, Chu T, Bowden W, Gassei K, Orwig K, et al. SOHLH1 and SOHLH2 coordinate spermatogonial differentiation. Dev Biol. 2012;361(2):301-12. Epub 2011/11/08. doi: 10.1016/j.ydbio.2011.10.027. PubMed PMID: 22056784; PubMed Central PMCID: PMCPMC3249242.
29. Chou DM, Adamson B, Dephoure NE, Tan X, Nottke AC, Hurov KE, et al. A chromatin localization screen reveals poly (ADP ribose)-regulated recruitment of the repressive polycomb and NuRD complexes to sites of DNA damage. Proc Natl Acad Sci U S A. 2010;107(43):18475-80. doi: 10.1073/pnas.1012946107. PubMed PMID: 20937877; PubMed Central PMCID: PMCPMC2972950.
30. Gong F, Chiu LY, Cox B, Aymard F, Clouaire T, Leung JW, et al. Screen identifies bromodomain protein ZMYND8 in chromatin recognition of transcription-associated DNA damage that promotes homologous recombination. Genes Dev. 2015;29(2):197-211. doi: 10.1101/gad.252189.114. PubMed PMID: 25593309; PubMed Central PMCID: PMCPMC4298138.
31. Yodh J. ATP-Dependent Chromatin Remodeling. Adv Exp Med Biol. 2013;767:263-95. doi: 10.1007/978-1-4614-5037-5_13. PubMed PMID: 23161016.
32. Kim Y, Fedoriw AM, Magnuson T. An essential role for a mammalian SWI/SNF chromatin-remodeling complex during male meiosis. Development. 2012;139(6):1133-40. Epub 2012/02/10. doi: 10.1242/dev.073478. PubMed PMID: 22318225; PubMed Central PMCID: PMC3283123.
33. Wang J, Gu H, Lin H, Chi T. Essential roles of the chromatin remodeling factor BRG1 in spermatogenesis in mice. Biol Reprod. 2012;86(6):186. Epub 2012/04/13. doi: 10.1095/biolreprod.111.097097. PubMed PMID: 22495890; PubMed Central PMCID: PMCPMC3386149.
34. Wang H, Zhao R, Guo C, Jiang S, Yang J, Xu Y, et al. Knockout of BRD7 results in impaired spermatogenesis and male infertility. Sci Rep. 2016;6:21776. Epub 2016/02/18. doi: 10.1038/srep21776. PubMed PMID: 26878912; PubMed Central PMCID: PMCPMC4754950.
35. Serber DW, Runge JS, Menon DU, Magnuson T. The Mouse INO80 Chromatin-Remodeling Complex Is an Essential Meiotic Factor for Spermatogenesis. Biol Reprod. 2016;94(1):8. doi: 10.1095/biolreprod.115.135533. PubMed PMID: 26607718; PubMed Central PMCID: PMCPMC4809561.
36. Dowdle JA, Mehta M, Kass EM, Vuong BQ, Inagaki A, Egli D, et al. Mouse BAZ1A (ACF1) is dispensable for double-strand break repair but is essential for averting improper gene expression during spermatogenesis. PLoS Genet. 2013;9(11):e1003945. doi: 10.1371/journal.pgen.1003945. PubMed PMID: 24244200; PubMed Central PMCID: PMCPMC3820798.

37. Broering TJ, Wang YL, Pandey RN, Hegde RS, Wang SC, Namekawa SH. BAZ1B is dispensable for H2AX phosphorylation on Tyrosine 142 during spermatogenesis. Biol Open. 2015;4(7):873-84. doi: 10.1242/bio.011734. PubMed PMID: 25979708; PubMed Central PMCID: PMCPMC4571090.
38. Thompson PJ, Norton KA, Niri FH, Dawe CE, McDermid HE. CECR2 is involved in spermatogenesis and forms a complex with SNF2H in the testis. J Mol Biol. 2012;415(5):793-806. doi: 10.1016/j.jmb.2011.11.041. PubMed PMID: 22154806.
39. Williams CJ, Naito T, Arco PG, Seavitt JR, Cashman SM, De Souza B, et al. The chromatin remodeler Mi-2beta is required for CD4 expression and T cell development. Immunity. 2004;20(6):719-33. Epub 2004/06/11. doi: 10.1016/j.immuni.2004.05.005. PubMed PMID: 15189737.
40. Peters AH, Plug AW, van Vugt MJ, de Boer P. A drying-down technique for the spreading of mammalian meiocytes from the male and female germline. Chromosome research. 1997;5(1):66-8. Epub 1997/02/01. PubMed PMID: 9088645.
41. Romer KA, de Rooij DG, Kojima ML, Page DC. Isolating mitotic and meiotic germ cells from male mice by developmental synchronization, staging, and sorting. Dev Biol. 2018;443(1):19-34. Epub 2018/08/28. doi: 10.1016/j.ydbio.2018.08.009. PubMed PMID: 30149006.
42. Oatley JM, Brinster RL. Spermatogonial stem cells. Methods Enzymol. 2006;419:259-82. Epub 2006/12/05. doi: 10.1016/S0076-6879(06)19011-4. PubMed PMID: 17141059.
43. Hammoud SS, Low DH, Yi C, Lee CL, Oatley JM, Payne CJ, et al. Transcription and imprinting dynamics in developing postnatal male germline stem cells. Genes Dev. 2015;29(21):2312-24. Epub 2015/11/08. doi: 10.1101/gad.261925.115. PubMed PMID: 26545815; PubMed Central PMCID: PMCPMC4647563.
44. Gassei K, Valli H, Orwig KE. Whole-mount immunohistochemistry to study spermatogonial stem cells and spermatogenic lineage development in mice, monkeys, and humans. Methods Mol Biol. 2014;1210:193-202. Epub 2014/09/01. doi: 10.1007/978-1-4939-1435-7_15. PubMed PMID: 25173170.

Figure Legends

Figure 1. CHD4 expression and formation of different NURD complexes during gametogenesis. (A) Expression of *Chd4* monitored by immunofluorescence in testis sections of 14dpp and 2 months (adult) old mouse using two distinct antibodies against CHD4, a rabbit polyclonal anti-CHD4 and anti-PLZF (top panel) and mouse monoclonal anti-CHD4 and anti-SOX9 (bottom panel). Arrows indicate examples of CHD4 positive spermatogonia (PLZF) or Sertoli (SOX9) cells. Cells within the punctuated line are pachytene spematocytes. **(B)** Spermatocyte chromosome spread obtained from two months old mouse testes immunostained with antibodies specific for CHD4, SYCP3, and

γH2AX (the last two markers of primary spermatocytes). Arrows indicate CHD4 signal at the X-Y pseudoautosomal region. This is a representative image obtained from the analysis of 3 different mice. **(C)** Western blot analysis of different NURD components in samples of cells enriched in undifferentiated spermatogonia (THY1.2+) (PLZF positive), differentiating spermatogonia (c-KIT+) (STRA8 positive), pachytene primary spermatocytes (SYCP3 positive) and the flow-through (FT) from the spermatogonia enrichment procedure, which contains mostly somatic cells, including a large amount of Sertoli cells (SOX9 positive). Lamin B (Lam B) and α-tubulin (Tub) were used as loading standards. The scheme represents the composition of a canonical NURD complex. **(D)** CHD4-participating NURD complexes in fractions enriched in spermatogonia or the flow-through cells assessed by coimmunoprecipitation with anti-CHD4 as a bait. Non-specific IgG was used as a bait control. Experiments were repeated twice, and the star marks an unspecific reactive band.

Figure 2. *Chd4* and *Chd3* gene targeting design and testis developmental defects in *Chd4* mutant mice. (A and B) Testis specific Cre knockout strategy for deletion of *Chd4* and *Chd3*. See description in Materials and Methods. **(C)** The panel shows expected time of expression for Ddx4-Cre used in this study. **(D)** In the top panel *Chd3* transcription levels were measured in Ddx4-*Chd3*$^{-/-}$ total testis and compared to wild type littermates (two months old mice, n=3). The lower panel show Chd4 transcription level in enriched fractions of spermatogonia obtained from 7dpp Ddx4-*Chd4*$^{-/-}$ and control wild type litter mate mice (mice, biological replicate n=3). **(E)** H&E-stained paraffin testis sections of wild type, Ddx4-*Chd4*$^{-/-}$, and Ddx4-*Chd3*$^{-/-}$ mice. Quantification of testis weight for wild type and homozygous knockout mice is also shown. Images and testis weigh measurements were obtained from three mice.

Figure 3. Ddx4-*Chd4*$^{-/-}$ mice show profound defects in gametogenesis. (A) H&E-stained histological sections of wild type and Ddx4-*Chd4*$^{-/-}$ testis. Stars mark seminiferous tubules with absent germ cells. Note unchanged number and morphology of Sertoli cells (indicated by green arrows). **(B)** Histological sections of wild type and Ddx4-*Chd4*$^{-/-}$ testis showing seminiferous tubules immunolabeled with SOX9 (a marker of Sertoli cells) and TRA98 (to mark germ cells). P, pachytene cells; Se, Sertoli cells; Rs, rounded spermatids. **(C)** H&E-stained histological sections of wild type and Ddx4-*Chd4*$^{-/-}$ ovaries. F, follicles and CL, corpora lutea.

Figure 4. Spermatogonia cell survival requires CHD4. (A) Histological sections of wild type and Ddx4-*Chd4*$^{-/-}$ testis cord from 9 days old mice stained with H&E (a and b) and Hematoxylin and immunostained with STRA8 antibodies (marking differentiating spermatogonia) (c and d). Arrows mark type of cells present in wild type but reduced in number or absent in the mutant. Experiments were done in at least three different mice showing similar results. **(B)** Immunostaining of sections of developing testis reveals severe loss of germ cells (TRA98) in *Chd4*$^{-/-}$ testis cords. **(C)** Quantitation of number of cell positive for TRA98, PLZF, and SOX9. 4dpp testis (PLZF, wild type, 9.9 ± 4.1, n=47 seminiferous tubules; *Chd4*$^{-/-}$ 2.2 ± 1.4, n=56, P<0.0001, t test. TRA98, wild type 12.6 ± 5.3, n=35; *Chd4*$^{-/-}$ *3.0* ± 1.9, n=37, P<0.0001, t test). 7dpp testes (PLZF, wild type, 14.6 ± 5.0, n=28; *Chd4*$^{-/-}$ 3.4 ± 2.4, n=45, P<0.0001, t test. TRA98, wild type 19.6 ± 5.9, n=48; *Chd4*$^{-/-}$ 3.0 ± 2.1, n=24, P<0.0001, t test). Experiments were done in three different mice showing similar results combined in our quantification. **(D)** Higher cell death in *Chd4*$^{-/-}$ knockout testes than in wild type controls at four days post-partum. Apoptotic cells were visualized by staining for TUNEL in three mice of each genotype. The percentage of apoptotic cells was counted only in the tubule cross-sections that contained apoptotic cells

and was normalized to total number of germ cells. 19.05 ± 11.17, n = 468 (mean ± SD, n= number of seminiferous tubules counted) wild type and 38.25 ± 13.72 *Chd4*$^{-/-}$, n = 344; P<0.0001 (two-tailed Student t test). The arrows indicate apoptotic cells and arrowhead non-apoptotic germ cells.

Figure 5. Effect of Chd4 deletion in Dmrt1 and Plzf expression. (**A**) Histological sections of wild type and Ddx4-*Chd4*$^{-/-}$ testis from 1, 4, and 7 dpp mice stained with CHD4 and DMRT1 antibodies. Arrows indicate examples of CHD4 positive spermatogonia (Wt) or CHD4 absence of staining in Ddx4-*Chd4*$^{-/-}$ spermatogonia and the correspondent cell stained for DMRT1. **(B)** Quantitation of fluorescence intensity of DMRT1 expression on spermatogonia is shown for wild type (Wt) and Ddx4-*Chd4*$^{-/-}$ knockout at ages of 1dpp (Wt = 82.17 ± 22.02, n=272; and KO = 37.20 ± 10.01, n=287, P<0.0001, Student t test) and 4dpp (Wt = 71.09 ± 20.93, n=242; and KO = 43.47 ± 14.88, n=198, P<0.0001, Student t test). Values represent the median fluorescence intensity ± standard deviation, n = total number of cells analyzed from 3 biological replicates using 3 different mice. (**C**) Histological sections of wild type and Ddx4-*Chd4*$^{-/-}$ testis from 1, 4, and 7dpp mice stained with antibodies against PLZF. **(D)** Quantitation of fluorescence intensity of PLZF expression on spermatogonia is shown for wild type and Ddx4-*Chd4*$^{-/-}$ knockout at ages of 1dpp (wt = 17.94 ± 4.10, n=300; and Ddx4-*Chd4*$^{-/-}$ = 10.89 ± 4.07, n=339, P<0.0001, Student t test) and 4dpp (Wt = 17.78 ± 4.70, n=282; and Ddx4-*Chd4*$^{-/-}$ = 9.11 ± 3.75, n=230, P<0.0001, Student t test). Values represent the median fluorescence intensity ± standard deviation, n = total number of cells analyzed from 3 biological replicates using 3 different mice. **(E)** Diagram representing CHD4, Dmrt1, and Plzf relationship in spermatogonia stem cell maintenance. Note that our studies do not address the possibility that Plzf may be a direct target of CHD4.

Figure 6. Impaired gamete development in Ngn3-*Chd4*$^{-/-}$ testis. (A) H&E-stained histological sections of wild type and Ngn3-*Chd4*$^{-/-}$ testis. Note the most advanced developmental stages marked by arrows. **(B)** Quantitation of wild type and Ngn3-*Chd4*$^{-/-}$ testis size. Compare mutant 0.026 ± 0.003, n = 6 mice (mean ± SD) with wild type 0.100 ± 0.008, n = 4 mice; P < 0.0001 (two-tailed Student t test). **(C)** Western blot showing CHD4 depletion in whole testis extract of 2 months old Ngn3-*Chd4*$^{-/-}$ mice testis (KO). **(D)** Expression of CHD4 in wild type and Ngn3-Chd4$^{-/-}$ testis assessed by immunofluorescence. Arrow indicates the presence of CHD4 at the sex body in pachynema (SYCP3/yH2AX staining). Arrowhead indicates the absence of CHD4 in zygotene-like cells of Ngn3-CHD4$^{-/-}$ testis. Similar results were observed in 3 different mice. **(E)** TUNEL-DAPI stained histological sections of wild type (1.87 ± 1.06, n = 62 seminiferous tubules) and Ngn3-*Chd4*$^{-/-}$ (4.68 ± 3.21, n = 142 seminiferous tubules; P < 0.0001, two-tailed t test) testis. **(F)** H&E-stained histological sections of wild type and Ngn3-*Chd4*$^{-/-}$ ovaries. F, follicles and CL, corpora lutea.

Figure 7. CHD4 deletion results in abnormal DNA repair and homologous chromosome synapsis. (A) Representative images of wild type and Ngn3-*Chd4*$^{-/-}$ spermatocytes immunostained with SYCP1, SYCP3, and γH2AX. Insets on the right show higher magnification of SYCP3 images. White arrow mark unsynapsed portions of chromosomes, blue arrows mark SYCP3 aggregates, and blue arrowheads mark examples of γH2AX outside the sex body. **(B)** Stages of meiosis of spermatocytes from wild type and Ngn3-*Chd4*$^{-/-}$ mice. Random spermatocytes were scored from 60 days old mice. **(C)** Quantitation of γH2AX signal outside the sex body in pachytene wild type and

zygotene-like Ngn3-*Chd4*$^{-/-}$ spermatocytes. **(D)** Quantitation of SYCP3 aggregates in wild type and Ngn3-*Chd4*$^{-/-}$ spermatocytes.

Figure 8. Diagram summarizing the proposed functions of CHD4 during premeiotic and meiotic stages of gametogenesis and the effect of *Chd4* deletion in testis development. Undiff Spg: undifferentiated spermatogonia, Diff Spg: differentiating spermatogonia, PI Spc: Pre-leptotene spermatocyte, Primary Spc: primary spermatocytes (leptotene-diplotene), Sec Spc: secondary spermatocyte.

Figure 1

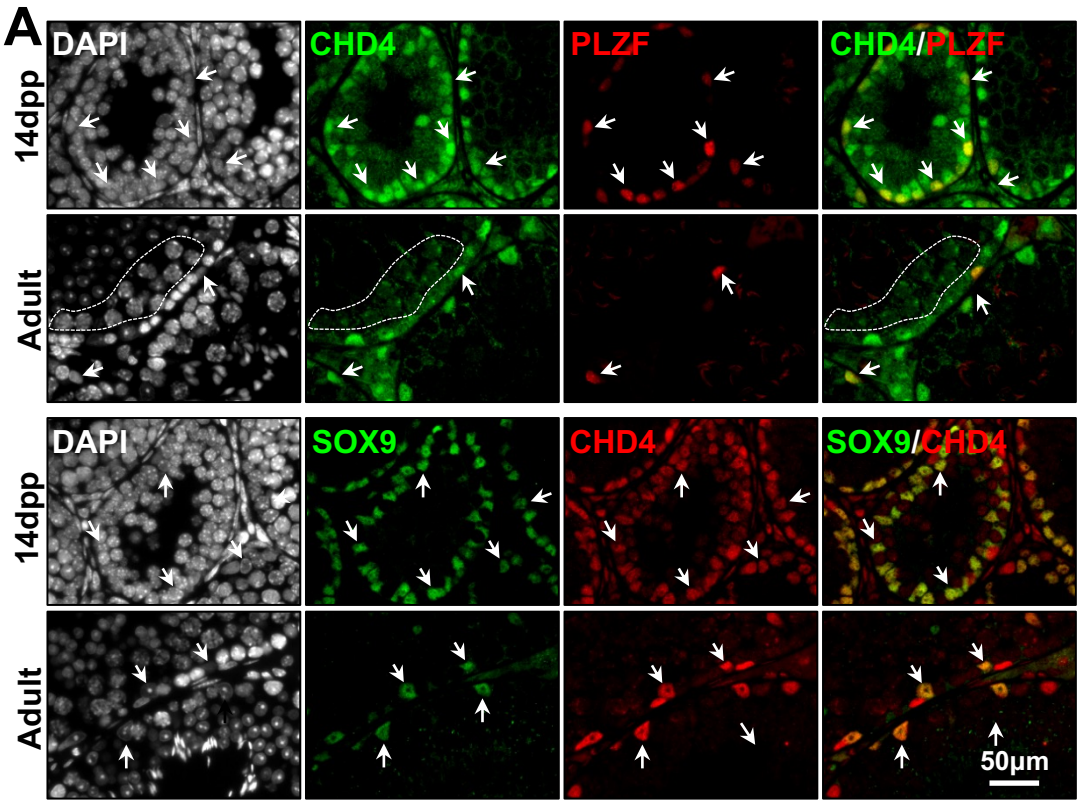
A
DAPI
CHD4
PLZF
CHD4/PLZF
14dpp
Adult
DAPI
SOX9
CHD4
SOX9/CHD4
14dpp
Adult
50μm

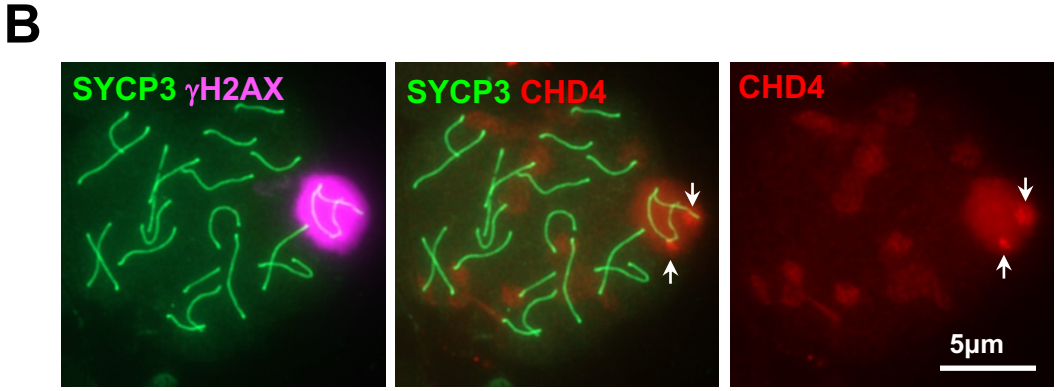
B
SYCP3 γH2AX
SYCP3 CHD4
CHD4
5μm

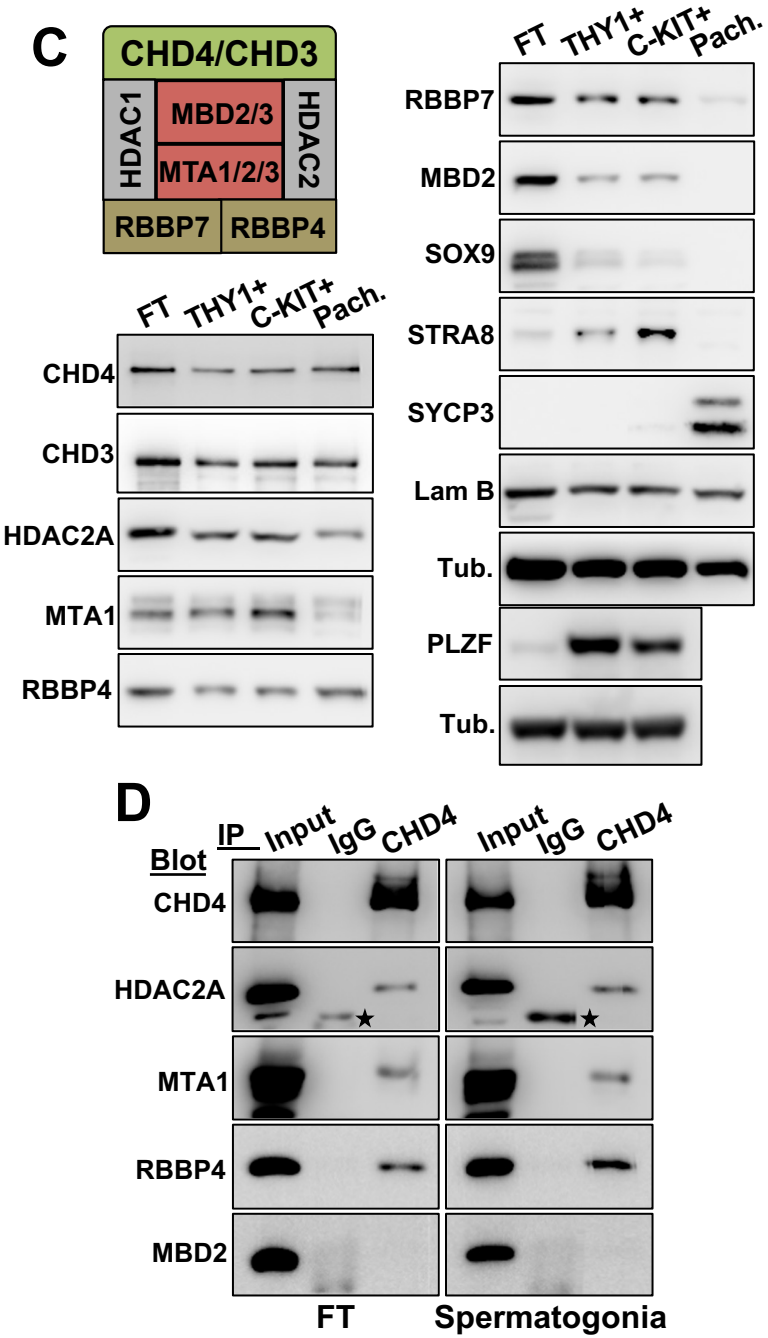
C
CHD4/CHD3
HDAC1
MBD2/3
HDAC2
MTA1/2/3
RBBP7
RBBP4
FT
THY1+
C-KIT+
Pach.
CHD4
CHD3
HDAC2A
MTA1
RBBP4
RBBP7
MBD2
SOX9
STRA8
SYCP3
Lam B
Tub.
PLZF
Tub.
D
IP
Input
IgG
CHD4
Input
IgG
CHD4
Blot
CHD4
HDAC2A
MTA1
RBBP4
MBD2
FT
Spermatogonia

Figure 2

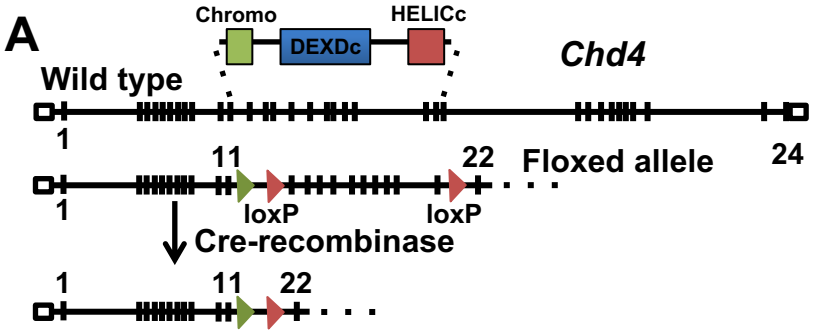
A
Chromo
HELICc
DEXDc
Chd4
Wild type
1
11
22
24
Floxed allele
1
loxP
loxP
Cre-recombinase
1
11
22

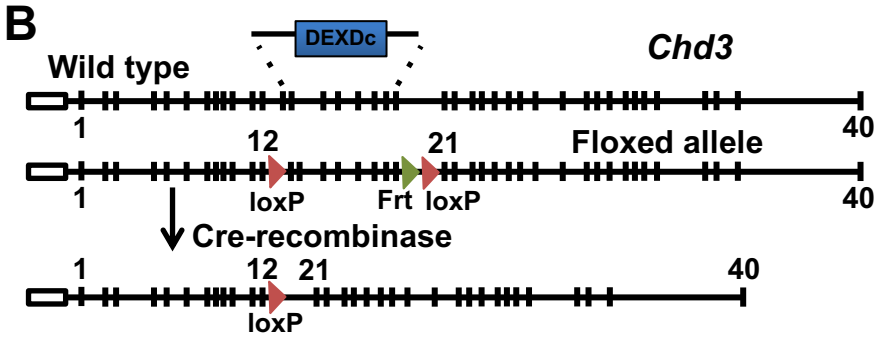
B
DEXDc
Chd3
Wild type
1
40
12
21
Floxed allele
1
loxP
Frt
loxP
40
Cre-recombinase
1
12
21
40
loxP

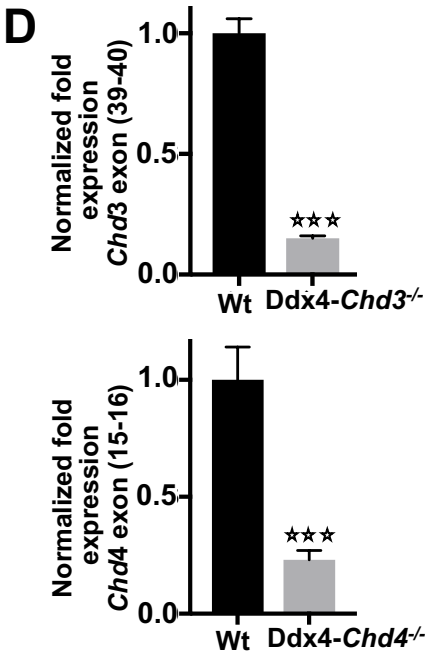
D
Normalized fold expression Chd3 exon (39-40)
1.0
0.5
0.0
***
Wt
Ddx4-Chd3-/-
Normalized fold expression Chd4 exon (15-16)
1.0
0.5
0.0
***
Wt
Ddx4-Chd4-/-

C
Primodial germ cells → Gonocytes → Spermatogonia → Spermatocytes
Mitosis
Meiosis
Ddx4-Cre

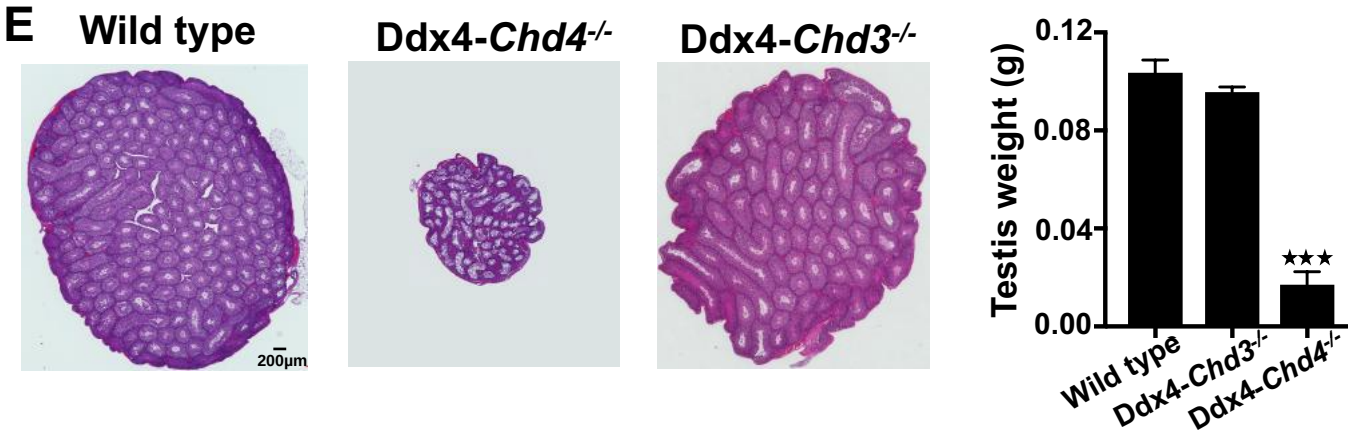
E
Wild type
Ddx4-Chd4-/-
Ddx4-Chd3-/-
200µm
Testis weight (g)
0.12
0.08
0.04
0.00
***
Wild type
Ddx4-Chd3-/-
Ddx4-Chd4-/-

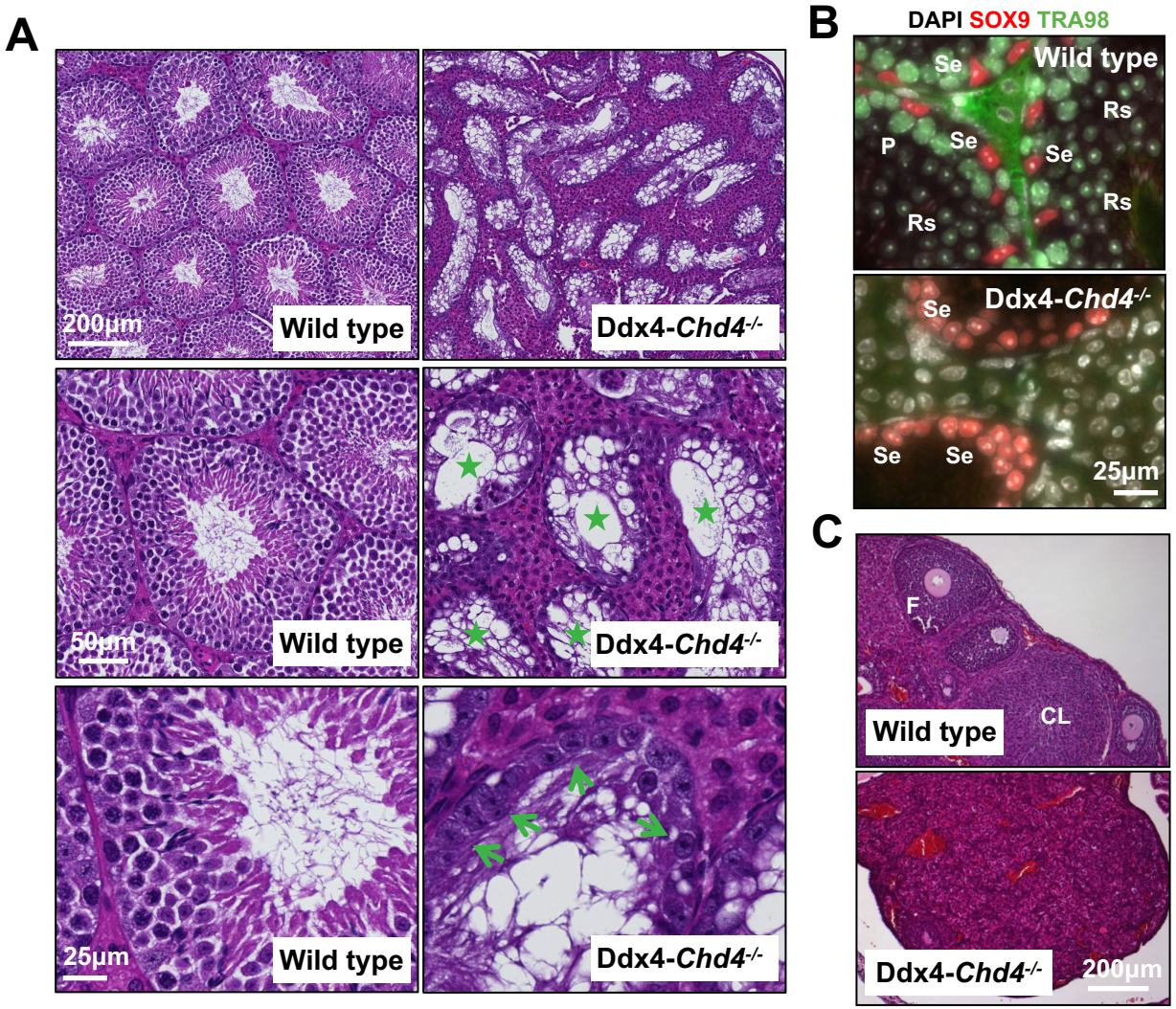
A
200μm
Wild type
Ddx4-Chd4-/-
50μm
Wild type
Ddx4-Chd4-/-
25μm
Wild type
Ddx4-Chd4-/-
B
DAPI SOX9 TRA98
Se
Wild type
Rs
P
Se
Se
Rs
Rs
Se
Ddx4-Chd4-/-
Se
Se
25μm
C
F
CL
Wild type
Ddx4-Chd4-/-
200μm

Figure 4

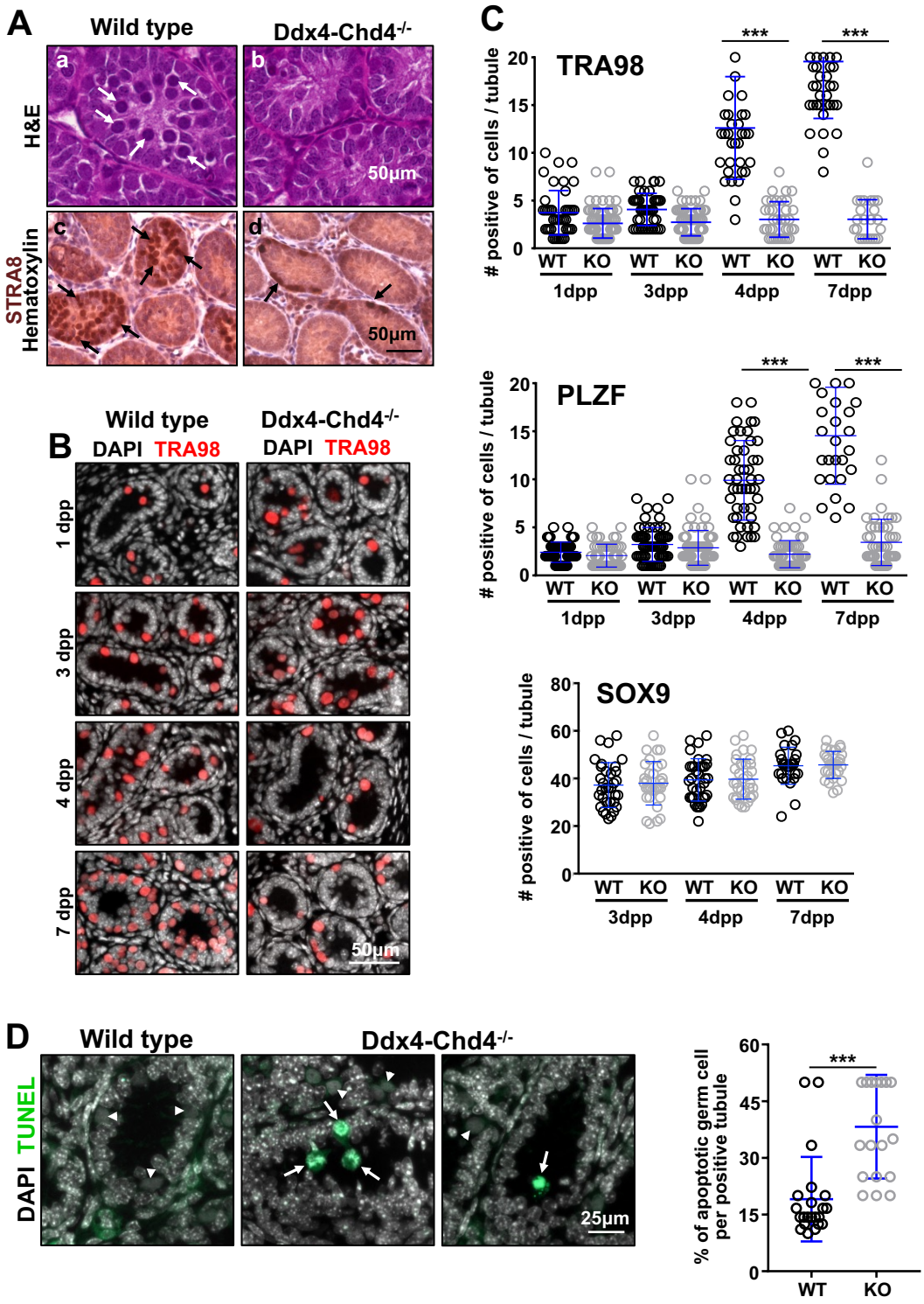
A
Wild type
Ddx4-Chd4-/-
H&E
STRA8
Hematoxylin
a
b
c
d
50µm
50µm
B
Wild type
Ddx4-Chd4-/-
DAPI TRA98
DAPI TRA98
1 dpp
3 dpp
4 dpp
7 dpp
50µm
C
TRA98
PLZF
SOX9
positive of cells / tubule
WT KO
1dpp
3dpp
4dpp
7dpp
***
D
Wild type
Ddx4-Chd4-/-
DAPI TUNEL
25µm
% of apoptotic germ cell per positive tubule
WT
KO
***

Figure 5

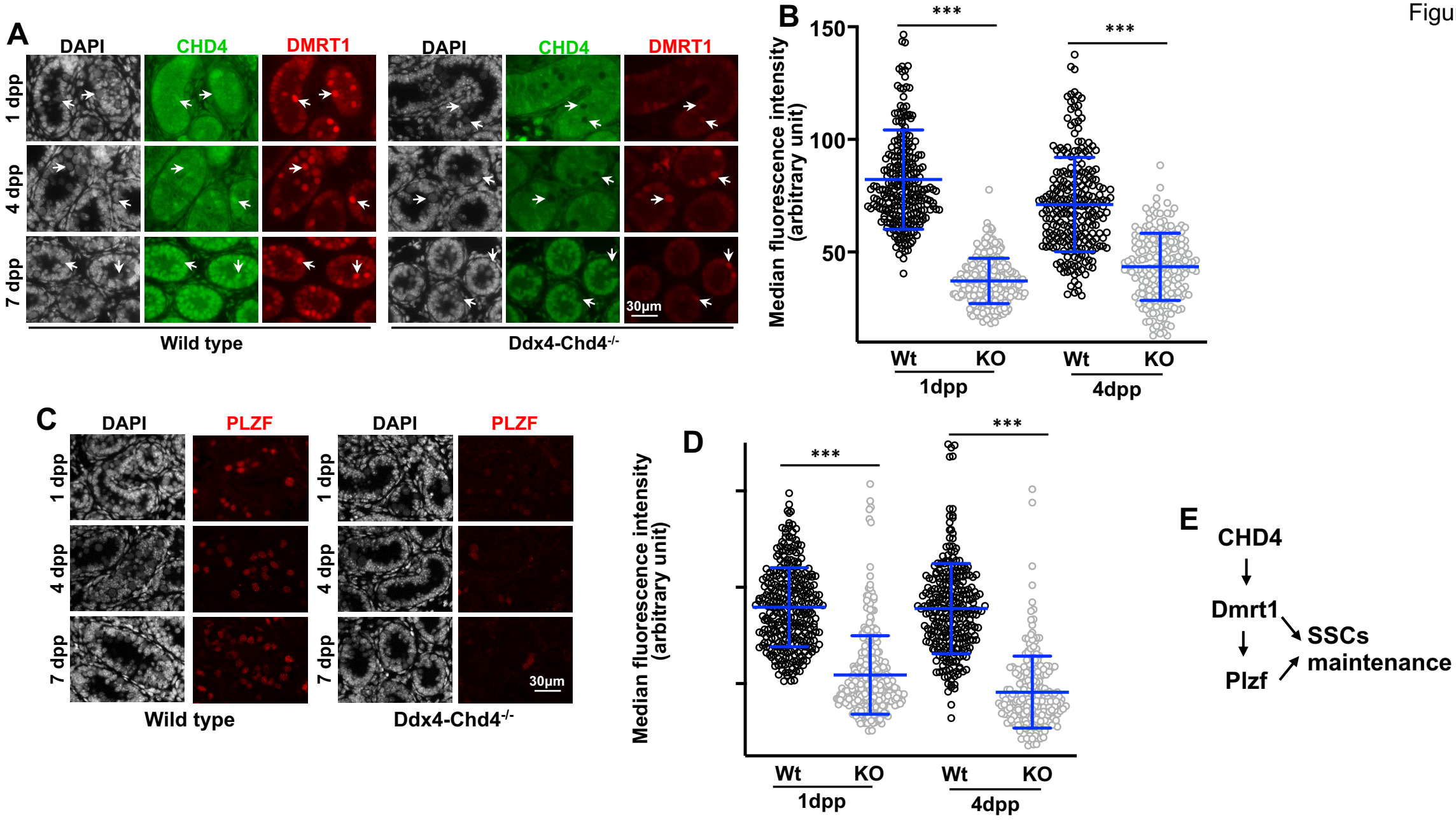
A
DAPI
CHD4
DMRT1
1 dpp
4 dpp
7 dpp
30μm
Wild type
Ddx4-Chd4-/-
B
Median fluorescence intensity (arbitrary unit)
150
100
50
***
Wt
KO
1dpp
4dpp
C
PLZF
D
E
CHD4
Dmrt1
Plzf
SSCs maintenance

Figure 6

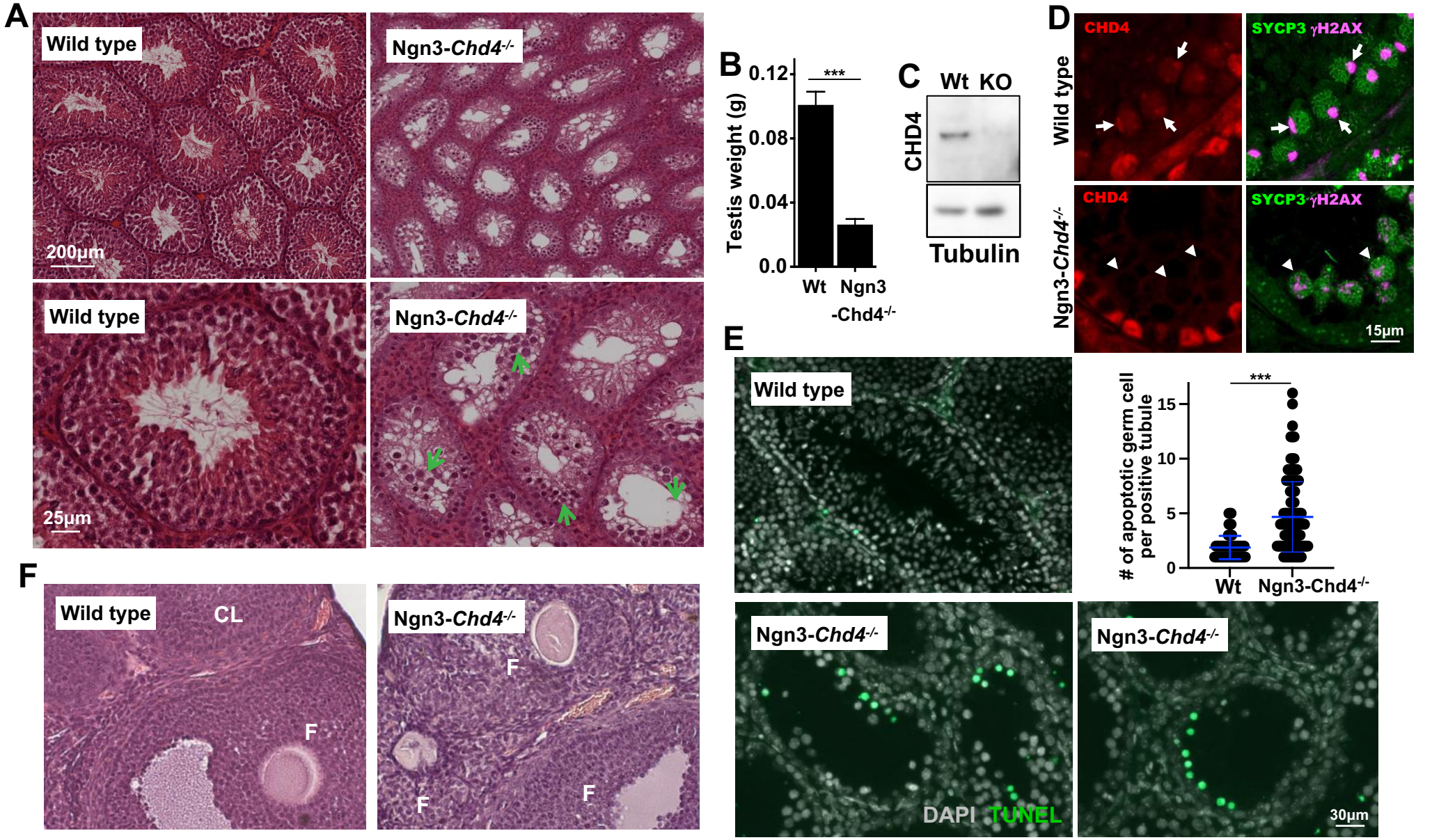
A
Wild type
Ngn3-Chd4-/-
200µm
Wild type
Ngn3-Chd4-/-
25µm
B
Testis weight (g)
0.12
0.08
0.04
0.0
***
Wt
Ngn3 -Chd4-/-
C
Wt KO
CHD4
Tubulin
D
CHD4
SYCP3 γH2AX
Wild type
Ngn3-Chd4-/-
15µm
E
Wild type
# of apoptotic germ cell per positive tubule
15
10
5
0
***
Wt
Ngn3-Chd4-/-
Ngn3-Chd4-/-
DAPI TUNEL
30µm
F
Wild type
CL
F
Ngn3-Chd4-/-
F
F
F

Figure 7

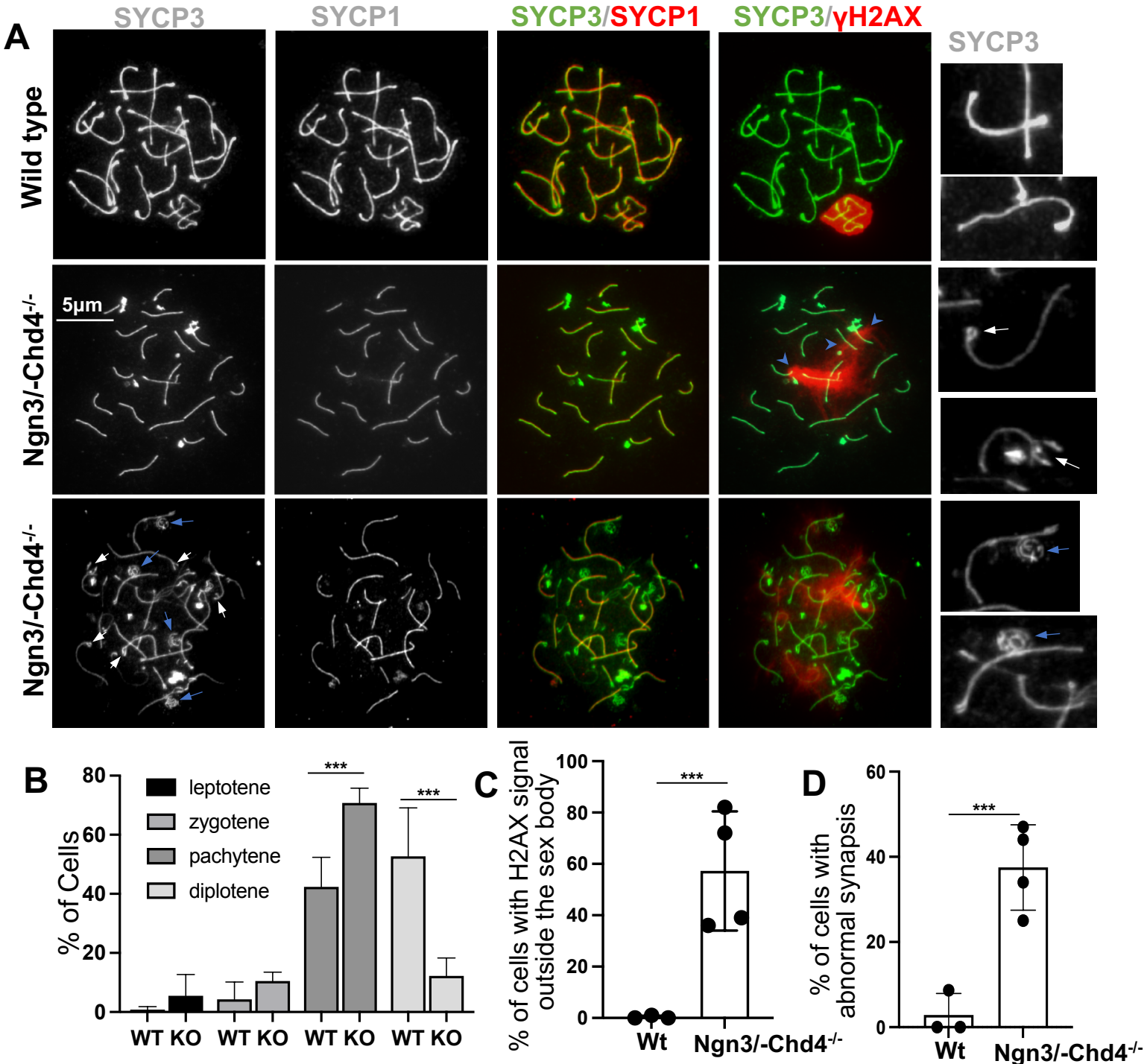
A
SYCP3
SYCP1
SYCP3/SYCP1
SYCP3/γH2AX
SYCP3
Wild type
Ngn3/-Chd4-/-
Ngn3/-Chd4-/-
5μm
B
leptotene
zygotene
pachytene
diplotene
% of Cells
80
60
40
20
0
***
***
WT KO
WT KO
WT KO
WT KO
C
% of cells with H2AX signal outside the sex body
100
80
60
40
20
0
***
Wt
Ngn3/-Chd4-/-
D
% of cells with abnormal synapsis
60
40
20
0
***
Wt
Ngn3/-Chd4-/-

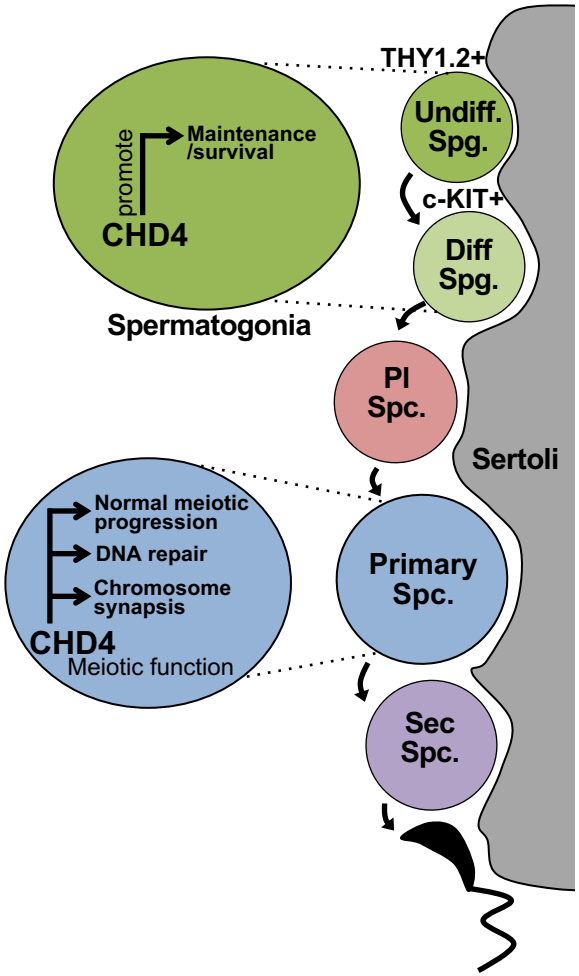
THY1.2+
Undiff.
Spg.
c-KIT+
Diff
Spg.
promote
Maintenance
/survival
CHD4
Spermatogonia
Pl
Spc.
Sertoli
Normal meiotic
progression
DNA repair
Chromosome
synapsis
CHD4
Meiotic function
Primary
Spc.
Sec
Spc.

Figure 8